Since January 2020 Elsevier has created a COVID-19 resource centre with free information in English and Mandarin on the novel coronavirus COVID-19. The COVID-19 resource centre is hosted on Elsevier Connect, the company's public news and information website.

Sensors & Actuators: B. Chemical 345 (2021) 130372

Contents lists available at ScienceDirect

Sensors and Actuators: B. Chemical

journal homepage: www.elsevier.com/locate/snb

Development of an ultrasensitive fluorescent immunochromatographic assay based on multilayer quantum dot nanobead for simultaneous detection of SARS-CoV-2 antigen and influenza A virus

Chongwen Wang [a,b,*,1], Xingsheng Yang [a,b,1], Shuai Zheng [a,b,1], Xiaodan Cheng [a,b], Rui Xiao [a,b,*], Qingjun Li [c], Wenqi Wang [a,b], Xiaoxian Liu [a,b], Shengqi Wang [b,*]

[a] College of Life Sciences, Anhui Agricultural University, Hefei, 230036, PR China
[b] Beijing Institute of Radiation Medicine, Beijing, 100850, PR China
[c] School of Pharmacy, Shandong University of Traditional Chinese Medicine, Jinan, 250355, PR China

ARTICLE INFO

Keywords:
Immunochromatographic assay
SARS-CoV-2
FluA
Simultaneous detection
Multilayer quantum dot

ABSTRACT

Rapid and accurate diagnosis of severe acute respiratory syndrome coronavirus 2 (SARS-CoV-2) and influenza A virus (FluA) antigens in the early stages of virus infection is the key to control the epidemic spread. Here, we developed a two-channel fluorescent immunochromatographic assay (ICA) for ultrasensitive and simultaneous qualification of the two viruses in biological samples. A high-performance quantum dot nanobead (QB) was fabricated by adsorption of multilayers of dense quantum dots (QDs) onto the SiO_2 surface and used as the highly luminescent label of the ICA system to ensure the high-sensitivity and stability of the assay. The combination of monodispersed SiO_2 core (~180 nm) and numerous carboxylated QDs formed a hierarchical shell, which ensured that the QBs possessed excellent stability, superior fluorescence signal, and convenient surface functionalization. The developed ICA biosensor achieved simultaneous detection of SARS-CoV-2 and FluA in one test within 15 min, with detection limits reaching 5 pg/mL for SARS-CoV-2 antigen and 50 pfu/mL for FluA H1N1. Moreover, our method showed high accuracy and specificity in throat swab samples with two orders of magnitude improvement in sensitivity compared with traditional AuNP-based ICA method. Hence, the proposed method is a promising and convenient tool for detection of respiratory viruses.

1. Introduction

The ongoing coronavirus disease 2019 (COVID-19) pandemic, which is caused by severe acute respiratory syndrome coronavirus 2 (SARS-CoV-2), has rapidly spread to over 214 countries since December 2019 and resulted in more than 104 million infected individuals and over 2.27 million deaths [1–3]. SARS-CoV-2 is spread through close person-to-person contact and has high infectiousness rate. The early symptoms (mainly cough and fever) of SARS-CoV-2 infection mimic those of common respiratory viruses, such as influenza A virus (FluA), influenza B virus (FluB), and respiratory syncytial virus (RSV) [4–6]; as such, controlling the epidemic spread and guiding clinical treatment are difficult. On another hand, FluA has received extensive attention for a long time because its spread causes seasonal epidemics and raging pandemic [7]. For example, the pandemic of 2009 (swine flu) was caused by FluA H1N1 strain (A/2009/H1N1) and resulted in more than 201,200 deaths [8]. Notably, recent report indicated patients with coinfecting FluA and SARS-CoV-2 have appeared [9,10]. Thus, methods for accurate and rapid diagnosis of FluA/SARS-CoV-2 are urgently needed.

To date, serological testing of virus specific immunoglobulins (e.g., IgM, IgG) in blood samples and direct detection of viral components (e.g., RNA or protein) are the two main strategies for diagnosis of respiratory virus infection [11–13]. Considering that the initial antibody responses to viral antigens are usually detected in the late stage of infection (7–14 days after virus exposure), serological antibody tests cannot achieve accurate screening of asymptomatic populations or early cases [14,15]. Current recommended methods for SARS-CoV-2 and FluA detection is real-time reverse transcription-polymerase chain reaction (RT-PCR) and immunoassays for antigens, such as enzyme-linked

* Corresponding authors at: Beijing Institute of Radiation Medicine, Beijing, 100850, PR China.
E-mail addresses: wangchongwen1987@126.com (C. Wang), ruixiao203@sina.com (R. Xiao), sqwang@bmi.ac.cn (S. Wang).
[1] These authors contributed equally to this work.

https://doi.org/10.1016/j.snb.2021.130372
Received 24 April 2021; Received in revised form 15 June 2021; Accepted 26 June 2021
Available online 29 June 2021

immunosorbent assay (ELISA) [16–19]. Although PCR and ELISA could provide accurate results with high specificity for respiratory tract specimens (nasal or throat swab) in the early stage of infection, the disadvantages include long processing time (>2 h) and tedious procedures, which severely limit their application in point-of-care testing (POCT) area.

Immunochromatographic assay (ICA) is a mature POCT technology with the merits of rapidity, low cost, portability, and simple operation and has been widely used in the field of food safety control, human health monitoring, and clinical diagnosis [20–24]. Developing an ICA-based method for respiratory virus is an ideal approach to improve the detection capability of SARS-CoV-2/FluA infections owing to the following advantages. First, this assay can be used directly to respiratory tract specimens without sample pretreatment steps and provide results quickly (generally 10−20 min). Second, the ICA strip is ready-to-use by ordinary people and can be applied to any public places, such as hospitals, communities, and schools, and is thus suitable for rapid screening virus of infected persons. Third, simultaneous detection of SARS-CoV-2/FluA in the ICA platform can be easily realized by setting two test (T) lines on the strip, thereby improving the detection efficiency. However, traditional ICA method has two inherent defects including limited sensitivity and poor quantitative ability due to the use of colloidal gold (AuNP)-based colorimetric analysis [25,26]. These defects hinder the large-scale implementation of ICA for respiratory virus diagnosis. In recent years, a new class of luminescent materials named quantum dot (QD) has been introduced into ICA systems to replace colorimetric labels [27–30]. These materials have advantages of high photostability, narrow fluorescence emission spectra, and strong luminescence. As such, QD nanoprobes can provide intense and quantifiable fluorescence signal for ICA. Moreover, QD beads (QBs) can be fabricated by encapsulating many QDs into a polymer or silica micelles, which can provide high luminescence and stability [31–35]. Thus, integrating high-performance QBs into an ICA system is likely to overcome the deficiencies of traditional ICA method and achieve sensitive detection of respiratory viruses.

Herein, we developed a two-channel fluorescent ICA method for ultrasensitive and simultaneous detection of SARS-CoV-2/FluA in real biological samples by using a novel silica-QD nanocomposite with triple-QD shell (SiTQD) as the advance signal probe. The innovations of the proposed SiTQD-ICA could be summarized in three points: (i) a novel QB label was fabricated for the first time by adsorption of three layers (thousands) of carboxylated QDs onto monodispersed 180 nm SiO_2 surface, which greatly enhanced the fluorescence signal of ICA; (ii) high-performance SiTQD QBs confer the ICA system with high stability and sensitivity for clinical sample testing; and (iii) a two-channel platform was established to simultaneously detect SARS-CoV-2 and FluA. The fluorescence signals of SiTQD labels on the two T lines could be easily observed using a UV light source for qualitative detection and quickly measured by a commercial fluorescent reader for quantitative analysis of SARS-CoV-2 and FluA. Under the optimal conditions, the sensitivity of SiTQD-ICA for detection of SARS-CoV-2 and FluA H1N1 reached 5 pg/mL and 50 pfu/mL, respectively. Moreover, the practical detection capability of the method was evaluated by testing inactivated SARS-CoV-2 samples. The specificity, accuracy, and stability of the proposed method were fully demonstrated, indicating the strong potential of SiTQD-ICA for POCT use.

2. Experimental section

2.1. Reagents and materials

Branched polyethyleneimine (PEI, MW ~25 kDa), tetraethyl orthosilicate (TEOS), N-hydroxy-sulfosuccinimide (sulfo-NHS), 2-(N-morpholino) ethanesulfonic (MES), N-(3-dimethylaminopropyl)-N′-ethylcarbodiimide hydrochloride (EDC), bovine serum albumin (BSA), and goat anti-mouse IgG antibody (Catalog#AP124) were purchased from Sigma–Aldrich (USA). CdSe/ZnS-COOH QDs (excitation/emission maxima ~365/625 nm) were supplied by Mesolight Inc. (Suzhou, China). Nitrocellulose (NC) membranes including CN95 and CN140 were purchased from Sartorius (Spain). Other ICA materials including sample pad, conjugate pad, polyvinyl chloride bottom plate, and absorption pad were supplied by Jieyi Biotechnology Co. (Shanghai, China).

The immunoreagents used for SARS-CoV-2 and FluA detection were commercial monoclonal antibodies (mAbs). The SARS-CoV-2 NP antigen (Catalog # 40588-V08B) and its capture mAb (Catalog#40143-R040) and detection mAb (Catalog#40143-MM08) were purchased from Sino Biological Inc. (China). FluA monoclonal capture mAb (Catalog#FluA-001) and detection mAb (Catalog# FluA-002) were obtained from Xinxin Bio, Ltd. (Jiangsu, China). Commercially available SARS-CoV-2 nucleocapsid detection ELISA Kit (Catalog #KIT40588) and Influenza H1N1 Hemagglutinin ELISA Kit (Catalog #KIT11055) were purchased from Sino Biological Inc. (Beijing, China). Influenza A (H1N1 2009/A) was supplied by our laboratory, which was cultured in chick embryo at 35 °C for 2 days, then quantified by plaque assay, and frozen at -70 °C until use [36]. Inactivated SARS-CoV-2 virions (~10^8 pfu/mL) were provided by courtesy of Prof. Chengfeng Qin's laboratory in the Beijing Institute of Microbiology and Epidemiology (Beijing, China) [37–39]. Human throat swab specimens were obtained from healthy volunteers from Beijing Institute of Radiation Medicine (Beijing, China), with the approval of Ethics Committee of the Institute.

2.2. Synthesis of SiO_2 NPs

SiO_2 NPs (~180 nm) were synthesized by a typical Stöber method with slight modification [40]. In brief, 1.6 mL of ammonia aqueous solution (28 wt%) and 2.4 mL of deionized water were mixed together in 40 mL of ethanol. The mixture was stirred with a magnetic stirrer at 600 r/min. After 2 min of stirring, 1.6 mL of TEOS was rapidly injected, and the mixture was continuously reacted for 3 h at 25 °C. The resulting SiO_2 NPs were collected by centrifugation (6000 rpm, 6 min), rinsed with ethanol twice, and dried at 70 °C in a vacuum oven.

2.3. Synthesis of SiO_2-QD nanocomposite with triple QD-shell

The SiTQD nanocomposite with a triple QD-shell was prepared via PEI-mediated LBL self-assembly. First, 1 mL of 180 nm SiO_2 NPs (1 mg/mL) was mixed with 40 mL of aqueous PEI solution (0.2 mg/mL) under vigorous sonication. After reaction for 50 min, PEI-coated SiO_2 NPs (SiO_2/PEI) were collected by centrifugation (6000 rpm, 6 min) and washed with deionized water twice. The formed SiO_2/PEI NPs were resuspended in 1 mL of deionized water and then mixed with 40 mL of CdSe/ZnS-MPA QDs (1 nM). The mixture was vigorously sonicated for 50 min at room temperature. During this process, the numerous CdSe/ZnS-MPA QDs were rapidly adsorbed on the SiO_2/PEI surface via electrostatic interaction. The formed SiO_2-QD core–shell nanocomposites (SiQD) were collected by centrifugation (5400 rpm, 6 min) and resuspended in 1 mL of deionized water. The PEI self-assembly and QD-adsorption processes were repeated. The SiDQD nanocomposite with dual QD shell and SiTQD nanocomposite with triple QD shell were sequentially fabricated. After coating of the third layer of QD, SiTQD nanocomposites were separated by centrifugation (4500 rpm, 6 min), washed once with deionized water, and resuspended in 10 mL of ethanol for future use.

2.4. Preparation of immuno-SiTQD labels

The SARS-CoV-2 NP antigen detecting antibody and FluA detecting antibody were conjugated with SiTQD NPs through carbodiimide chemistry. Briefly, 1 mL of prepared SiTQD NPs were separated from ethanol and activated via immersion in 0.5 mL of MES solution (0.1 M) containing 1 mM EDC and 2 mM sulfo-NHS under sonication. After 15

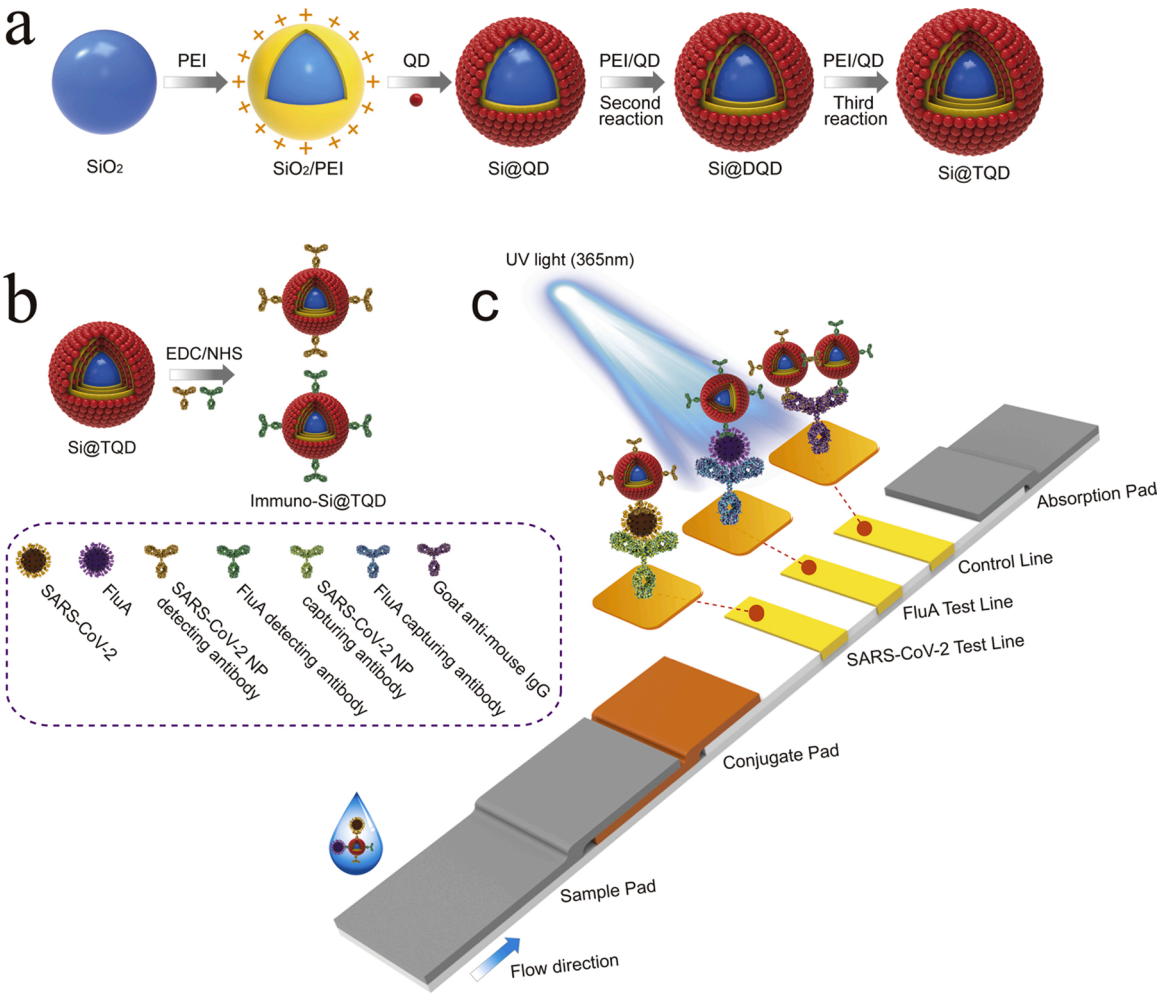

Scheme 1. Fabrication of SiTQD probes and their application to ICA-based biosensor for simultaneous detection of SARS-CoV-2 and FluA. (a) Synthesis of SiTQD nanocomposite, (b) preparation of immuno-SiTQD probes, and (c) operating principle of SiTQD-ICA strip for detecting two target respiratory viruses.

min, the activated SiTQD NPs were collected by centrifugation (4,500 rpm, 6 min) and redispersed in 0.2 mL of PBS solution (0.1 mM, pH7.4). The mixture was reacted with 15 μg of detecting antibodies for 2 h, followed by surface blocking with 100 μL of 10 % BSA for another 1 h. Finally, immuno-SiTQD labels were collected by centrifugation (4200 rpm, 6 min), washed once with PBS, redispersed in 1 mL of PBS solution containing 0.5 % sucrose (w/v), 0.5 % BSA (w/v), 0.02 % NaN_3 (w/v), and 0.05 % Tween 20 (v/v), and stored at 4 °C.

2.5. Preparation of the two-channel ICA strip

The two-channel ICA strip was consisted of a sample pad, a conjugate pad containing two specific immuno-SiTQD labels, a NC membrane with two test lines (T lines) and one control line (C line), and an absorbent pad. The conjugate pad was first impregnated with 0.1 M PBS containing 0.05 % Tween 20 and completely dried at 37 °C for 12 h. In brief, 100 μL of anti-SARS-CoV-2 NP mAb-modified SiTQD and 100 μL of anti-FluA mAb-modified SiTQD were mixed in a 1:1 ratio and then evenly sprayed onto the conjugate pad. The two T lines and the C line were constructed on the NC membrane by spraying the SARS-CoV-2 NP capturing antibody (1.6 mg/mL), FluA capturing antibody (0.8 mg/mL), and goat-anti-mouse IgG antibody (1 mg/mL) with a constant dispense of 0.1 μL/mm by the XYZ spraying platform (Biodot, USA). All the ICA components were placed into a drying oven at 37 °C for 4 h and then attached onto the plastic backing card in sequence. The assembled ICA card was cut into 3 mm-wide strips and preserved in desiccator until use.

2.6. Analytical procedure for simultaneous detection of SARS-CoV-2/FluA

The testing processes for inactivated SARS-CoV-2 virion and active FluA H1N1 viruses were carried out inside a Class II biological safety cabinet. First, the concentration of FluA H1N1 sample was determined via the classical plaque assays, and the results were displayed in Fig. S1. Then, the concentration-determined H1N1 virion (1×10^8 pfu/mL) were prepared according to the results of plaque assays. After that, a series of throat swab samples containing different concentrations of FluA H1N1 was prepared to assess the analytical performance of the proposed ICA strip for real samples. Briefly, 40 μL of the prepared samples were mixed with 40 μL of running buffer. The mixture was vortexed and pipetted onto the sample pad of ICA strip. After 15 min of chromatography, the fluorescence signal on the two T zones and C line was observed using a UV light. The quantitative analysis of two target respiratory viruses was realized by recording the fluorescence intensities of the two T lines. After the use of SiTQD-ICA strip, the tested strips were collected and treated with a steam pressure of 120 °C for 30 min, and then disposed of as potentially biohazardous waste.

3. Results and discussion

3.1. Fabrication and characterization of SiTQD QBs

Scheme 1a illustrates the preparation of multilayer SiTQD QBs based

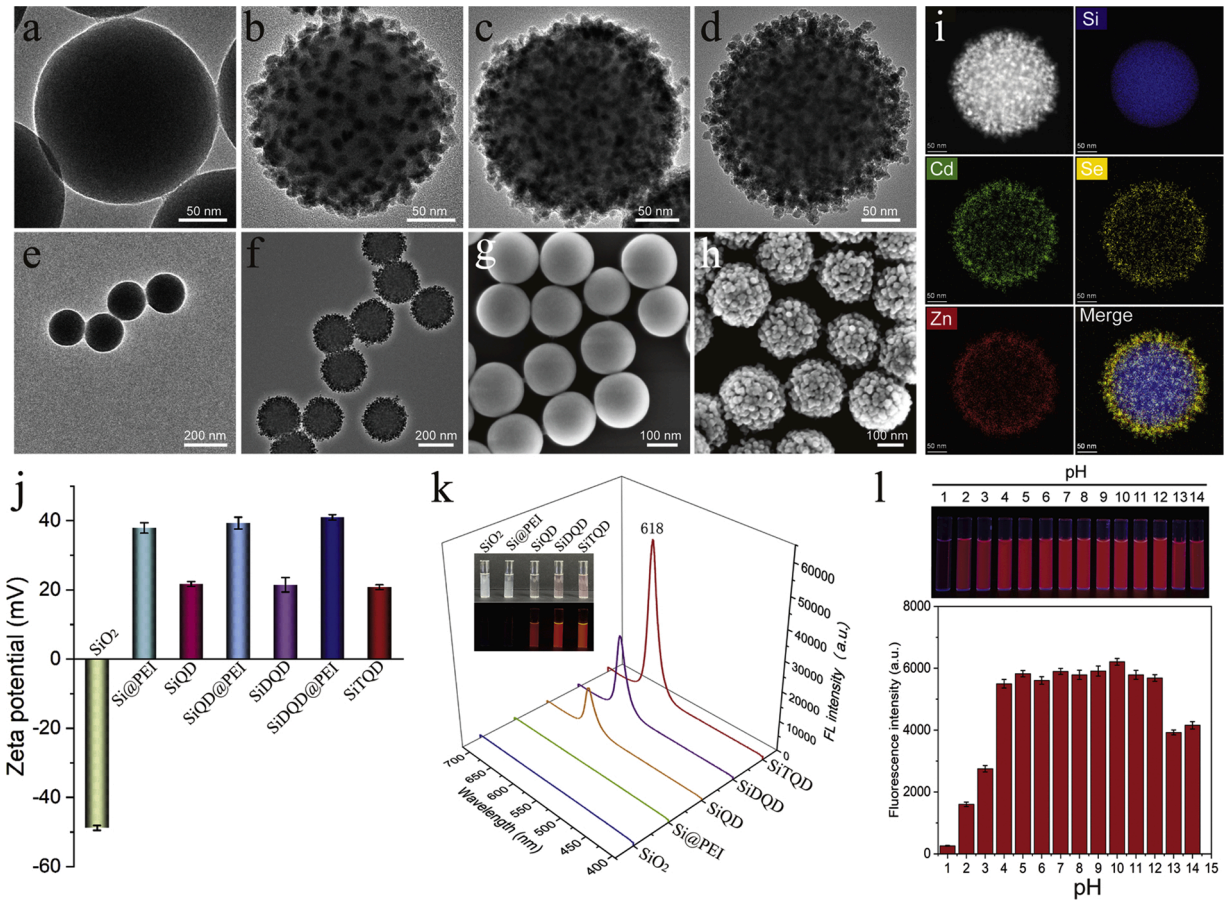

Fig. 1. Characterization of the fabricated SiTQD nanocomposite. TEM images of (a) single SiO_2 core, (b) SiQD, (c) SiDQD, and (d) SiTQD nanocomposite. TEM images of multiple (e) SiO_2 NPs and (f) SiTQD NPs, and their corresponding SEM images (g) and (h), respectively. (i) EDS elemental (Si, Cd, Se, Zn) mapping images of a SiTQD NP. Zeta potentials (j) and fluorescence emission spectra (k) of the synthesized NPs from each stage. The inset in (k) displays the photographs of these NPs solution under visible (upper) and UV light (lower). (e) Fluorescence images and intensities of SiTQD at different pH values. (l) Photograph of SiTQD NPs at various pH values under UV light (upper) and their corresponding fluorescence intensities at maximum emission wavelength (lower).

on a layer-by-layer (LbL) assembly strategy via PEI-mediated electrostatic adsorption of three layers of QDs onto the surface of SiO_2 sphere. The high-performance SiTQD QBs were introduced into the two-channel ICA instead of the common QD with the following characteristics: (i) a ~180 nm SiO_2 core as the monodispersed supporter to provide hydrophilicity and colloidal stability; (ii) a triple-layer QD shell containing thousands of QDs to generate high luminescence; and (iii) abundant surface carboxyl groups for convenient surface functionalization.

The fabricated SiTQD QBs were characterized by transmission electron microscopy (TEM) and scanning electron microscopy (SEM). Fig. 1a–d display the high-resolution TEM images of SiO_2, SiQD, SiDQD with dual QD shell, and SiTQD with triple QD shell, respectively. The prepared SiO_2 sphere (~180 nm) exhibited a spherical morphology with a smooth surface (Fig. 1a). Our previous works indicated the cationic PEI could directly coat onto the SiO_2 surface through ultrasonic driving [41]. As observed in Fig. S2, the transparent PEI layer with thickness of about 2.4 nm was successfully wrapped around the SiO_2 core under 50 min sonication. The positively charged SiO_2@PEI NPs were immersed in QDs solution with excess carboxylated CdSe/ZnS QDs and quickly absorbed many QDs onto their surface by electrostatic interaction. As shown in Fig. 1b, dense QDs (~12 nm) spread uniformly on the surface of SiO_2@PEI after the first round of QDs adsorption. The formed SiQD as the template was repeatedly reacted with positive polymer PEI and negatively charged QDs to build multiple-layer QD-coated silica nanocomposite.

With the successive adsorption of dual and triple layers of QD, the resulting SiDQD with dual QD shell (Fig. 1c) and SiTQD with triple QD shell (Fig. 1d) were successfully fabricated. The TEM images indicated that the number of QDs loaded onto the SiO_2 surface increased obviously with the number of PEI-driven assembly, and numerous QDs densely covered the SiTQD surface to form a hierarchical structure. The average diameter of SiTQD QB increased to approximately 240 nm after triple-QD shell formation (Fig. S3). The maximum loading amount of QDs for SiQD, SiDQD, and SiTQD were calculated to be approximately 923, 2050, and 3400, respectively (Supporting information S1/Fig. S4). Importantly, the SiO_2, PEI, and carboxylated QDs were hydrophilic materials, thereby ensuring the excellent dispersity of SiTQD nanocomposites. Fig. 1e-f reveal that the SiTQD NPs possess high monodispersity as well as SiO_2 spheres. The SEM images in Fig. 1g and h showed the surface morphology of SiTQD before and after QDs adsorption. The SiTQD surface became rough, which provided large surface site and benefitted antibody conjugation.

We employed energy-dispersive X-ray spectroscopy (EDS) mapping for analysis of the elemental distributions in SiTQD. As revealed in Fig. 1i, dense Cd, Se, and Zn were well distributed outside of the Si core, which clearly exhibited the layered shell structure of SiTQD. Moreover, the variations in the zeta potentials of nanocomposites revealed the synthetic principle of SiTQD. As shown in Fig. 1j, the zeta potential of SiO_2-based nanocomposites increased sharply after PEI coating and decreased obviously after carboxylated QDs adsorption. The LbL assembly of the three layers of PEI and QDs resulted in the zeta potential values of -48.8, 37.9, 24.6, 39.3, 22.5, 41.2, and 22.8 mV for SiO_2/PEI, SiQD, SiQD/PEI, SiDQD, SiDQD/PEI, and SiTQD, respectively. Such regular changes in zeta potential confirmed that the fabrication of

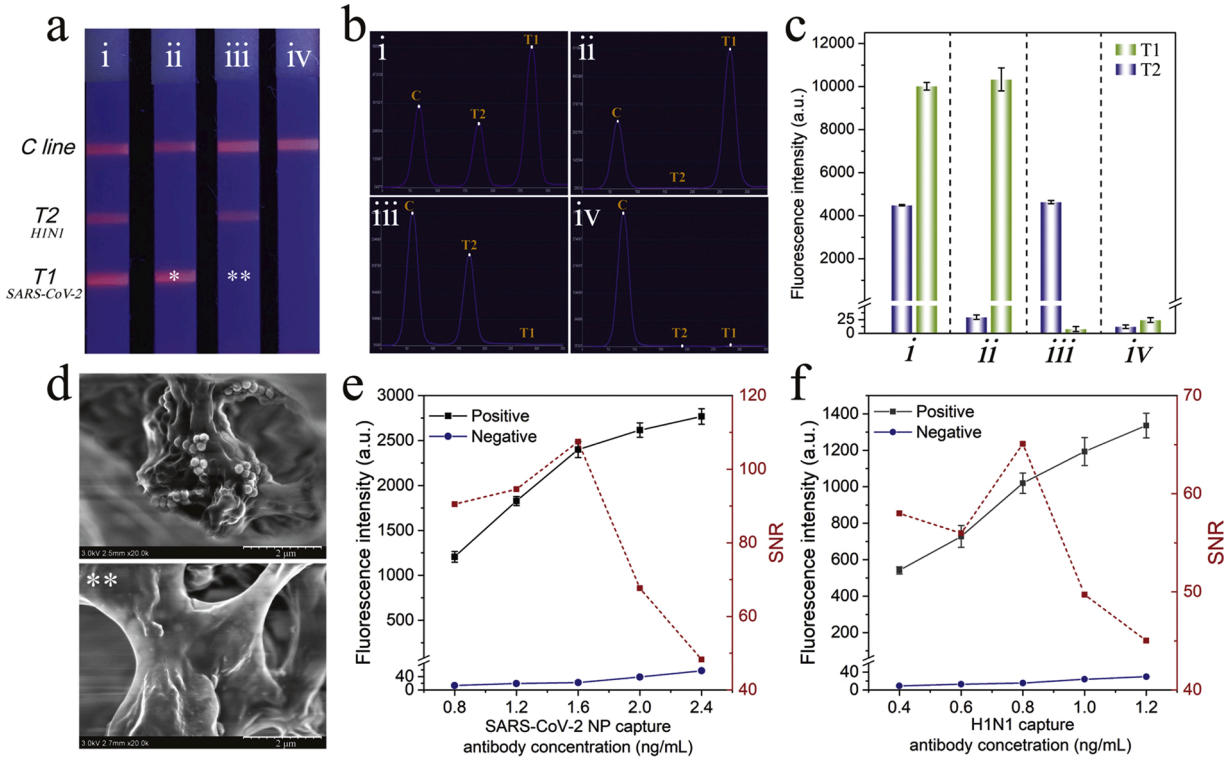

Fig. 2. (a) Photograph, (b) corresponding scanning waveforms of fluorescence, (c) fluorescence intensity of SiTQD-based ICA with different concentration of SARS-CoV-2 NP antigen and FluA H1N1: (i) 10 ng/mL, 10^4 pfu/mL; (ii) 10 ng/mL, 0 pfu/mL; (iii) 0 ng/mL, 10^4 pfu/mL; and (iv) 0 ng/mL, 0 pfu/mL. (d) Typical SEM images of the test zone for SARS-CoV-2 NP antigen concentrations of 10 ng/mL (*) and 0 ng/mL (**). Optimization of (e) SARS-CoV-2 NP capture antibody and (f) FluA capture antibody concentration on the T line. The error bars showed standard deviations calculated from three tests.

SiTQD was driven by PEI-mediated electrostatic adsorption [42].

The practical sensing capability of SiTQD NCs was assessed by systematically studying their optical property and colloidal stability. The photographs and fluorescence spectra of the SiO_2-based NCs are displayed in Fig. 1k. The SiO_2 and SiO_2@PEI exhibited no obvious fluorescence signal, whereas NCs with one to triple QD shells all showed bright red fluorescence. By measuring signal intensity of the major emission peak at ~618 nm, the luminescence of SiTQD was 3.58 and 1.76 times higher than those of SiQD and SiDQD, respectively, due to the larger amount of loaded QDs of the triple QD shell. The SiTQD exhibited excellent stability due to the highly stable SiO_2 core. As revealed in Fig. S5, the fluorescence intensity of SiTQD was unaffected by the high-salt environment and long-term preservation. Moreover, the SiTQD showed stable fluorescence intensity in aqueous samples over a wide range of pH values of 4–12 (Fig. 1l). The superior fluorescence properties and stability of SiTQD ensured its wide applications in complex samples.

3.2. Construction of SiTQD-based ICA

Two kinds of immuno-SiTQD labels for two target respiratory viruses and an ICA strip with two test lines were prepared for simultaneous detection of SARS-CoV-2 and FluA, as illustrated in Scheme 1b and c, respectively. The triple layers of carboxylated QDs formed shell of SiTQD, providing not only sufficient carboxyl groups for antibody conjugation but also larger external surface area than the common QD with smooth shell, thereby increasing the efficiency of antibody coupling. Using the carbodiimide cross-linking method [43], the SARS-CoV-2 NP monoclonal antibody and FluA monoclonal antibody were directly immobilized on the surface of SiTQD, respectively. As indicated in Fig. S6, the zeta potential values of immuno-SiTQD significantly declined after the antibody coupling and remained stable at -13.2 and -18.6 mV by reacting with 15 μg of the SARS-CoV-2 NP and FluA detection antibody, respectively. These results verified that the amount of antibody conjugated onto the SiTQD surface was saturated. The two-channel ICA for SARS-CoV-2/FluA detection was constructed by integrating five parts into a strip, including a sample pad, an absorbent pad, a conjugate pad containing two immuno-SiTQD labels, two separate test lines (T1 and T2) to coat the SARS-CoV-2 NP mAb and FluA mAb, and a control zone to coat goat anti-mouse IgG. As illustrated in Scheme 1c, the detection process of SiTQD-ICA was carried out via one step. When the test sample was added dropwise onto the sample pad, the solution migrated toward the absorbent pad via capillary action and rehydrated the immuno-SiTQD labels on the conjugate pad. During this process, the SARS-CoV-2 NP or FluA bind tightly to the SiTQD labels by antibody–antigen reaction. Upon reaching the T zones (T1/T2), the formed SiTQD/virus immunocomplexes were immobilized by the corresponding T lines that coated SARS-CoV-2 and FluA capture mAbs, resulting in detectable fluorescence signal on the T lines. In theory, higher concentration of target virus results in higher fluorescence intensity of corresponding T line. The excess immuno-SiTQD will reach the C line and caught by goat anti-mouse IgG, which can determine the validity of the assay.

The designed ICA biosensor for target virus detection was based on the formation of specific sandwich immunocomplexes via antigen–antibody interaction on the test line. Therefore, suitable antibodies with affinity and specificity are the key to construct the two-channel ICA. Our previous work screened a pair of efficient mAbs for FluA detection [44]. The SARS-CoV-2 NP mAbs used in this study were selected as shown in Fig. S7. In addition, some important parameters of paper chromatography strip with big nanotags (~200 nm) were well studied in our previous works [45–47]. From these experiences, the NC membrane type and running buffer ingredient needed to be first optimized because they are closely related to the transport of SiTQD/virus complexes on the strip. As revealed in Fig. S8a, using the CN140 membrane with 8 μm pore size achieved the highest signal-to-noise ratio (SNR) for detection of both target viruses. NP-40 was added into the

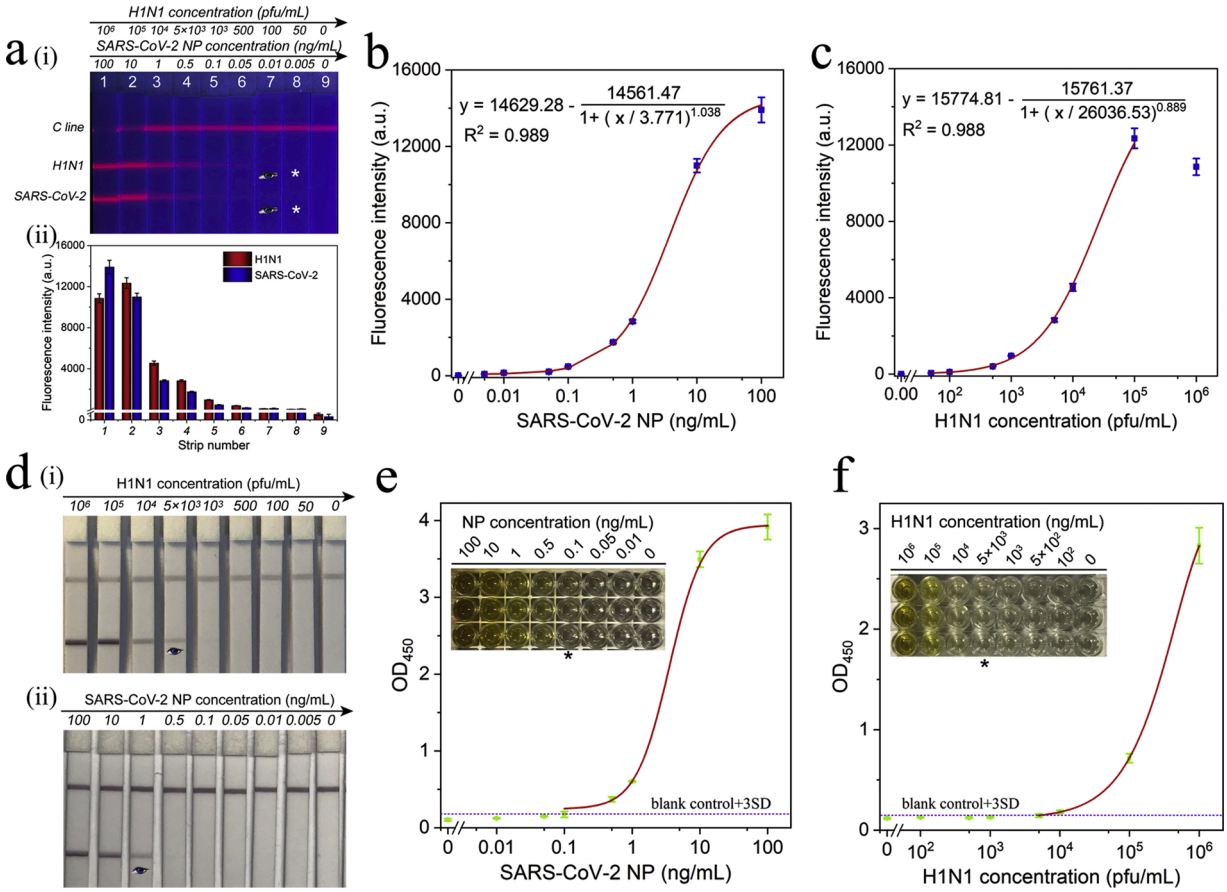

Fig. 3. (a) Fluorescence pictures (i) and corresponding test line intensities (ii) of SiTQD-based ICA strip for SARS-CoV-2 NP antigen and H1N1 detection. Corresponding calibration curves for (b) SARS-CoV-2 NP antigen and (c) H1N1. The error bars represented standard deviations calculated from three experiments. (d) Photographs of colloidal gold-based ICA strips for different concentrations of (i) H1N1 and (ii) SARS-CoV-2 NP antigen detection. (e-f) ELISA analysis for SARS-CoV-2 NP antigen (e) and H1N1 detection (f). The insets are colorimetric results of ELISA plates for different concentrations of target virus antigens.

running buffer to effectively lyse the SARS-CoV-2 virion and fully release the NP antigen [48]. Fig. S8b shows that the PBS buffer (10 mM, pH 7.4)-based running buffer containing 1% Tween 20, 0.5 % NP-40, and 1% BSA reduced the non-specific adsorption of SiTQD labels and maximized SNR on the test line.

The capture mAbs (0.8 mg/mL) for SARS-CoV-2 NP antigen and FluA was sprayed on CN140 membrane to set the two T lines (T1 for SARS-CoV-2 and T2 for FluA) to evaluate the multiplex detection ability of SiTQD-ICA. The prepared two-channel ICA was used to detect samples containing different concentrations of SARS-CoV-2 NP antigen and FluA H1N1. As shown in Fig. 2a, the fluorescence image of the ICA strip for the sample containing SARS-CoV-2/H1N1 exhibited two bright fluorescence T lines, whereas only one fluorescence band appeared in the T zone for SARS-CoV-2 or H1N1. No visible fluorescence T line was found in the strip for blank control group, and no cross reaction occurred between the two T lines in all tested strips, suggesting the good selectivity of the two-channel ICA biosensor. The corresponding fluorescence spectra and detailed intensity values of the tested strips were easily measured by utilizing a commercial fluorescent instrument, as displayed in Fig. 2b and c, respectively. The intensities of the obtained fluorescence signal of T lines were consistent with the naked eye observation and more beneficial for quantitative determination. The SEM images taken from ICA strips verified that many SiTQD labels were caught on the T line for positive sample, while no observable SiTQD attached on the same zone for negative control (Fig. 2d). All these results confirmed that the proposed SiTQD-ICA could be a feasible method for simultaneous and quantitative detection of SARS-CoV-2/FluA by measuring the fluorescence signals of two T lines. The concentration of capture mAbs loaded on the T lines was optimized to further improve the sensitivity of SiTQD-ICA. As shown in Fig. 2e-f, 1.6 mg/mL mAb for SARS-CoV-2 and 0.8 mg/mL of mAb for FluA loaded on the T1 and T2 lines, respectively, achieved the highest SNR of the fluorescence intensity. In addition, the optimal reaction time of ICA was investigated by analysis the SNR value of T lines during the chromatography process. As revealed in Fig. S9, 15 min of chromatography time was enough for quantitative detection of two target viruses via SiTQD-ICA.

3.3. *Analytical performance of the two-channel SiTQD-ICA*

Under the optimal conditions, the detection performance of SiTQD-ICA for clinical specimens was evaluated by detecting a series of throat swab samples spiked with different conditions of SARS-CoV-2 NP and H1N1. As shown in the fluorescence image of ICA strips in Fig. 3a(i), the red fluorescence bands on the test lines became brighter with increasing concentrations of the SARS-CoV-2 NP/H1N1 in the wide detection ranges of 0.01–100 ng/mL and 100–10^5 pfu/mL, respectively. The fluorescence test lines for 0.01 ng/mL of SARS-CoV-2 and 100 pfu/mL of H1N1 were clearly distinguished from those of negative control by the naked eye. Notably, an obvious “hook effect” [49,50] was observed at the T2 line for 10^6 pfu/mL of H1N1, but this phenomenon did not affect the qualitative detection of H1N1. Quantitative analysis of target viruses was conducted by reading the fluorescence intensity of T1/T2 lines. The corresponding fluorescence intensities of T1/T2 lines are displayed in Fig. 3a(ii). Based on the fluorescent ICA values, the calibration curves for SARS-CoV-2 NP and FluA H1N1 were plotted in Fig. 3b and c. The IUPAC protocol ($LOD = y_{blank} + 3\,SD_{blank}$) was applied

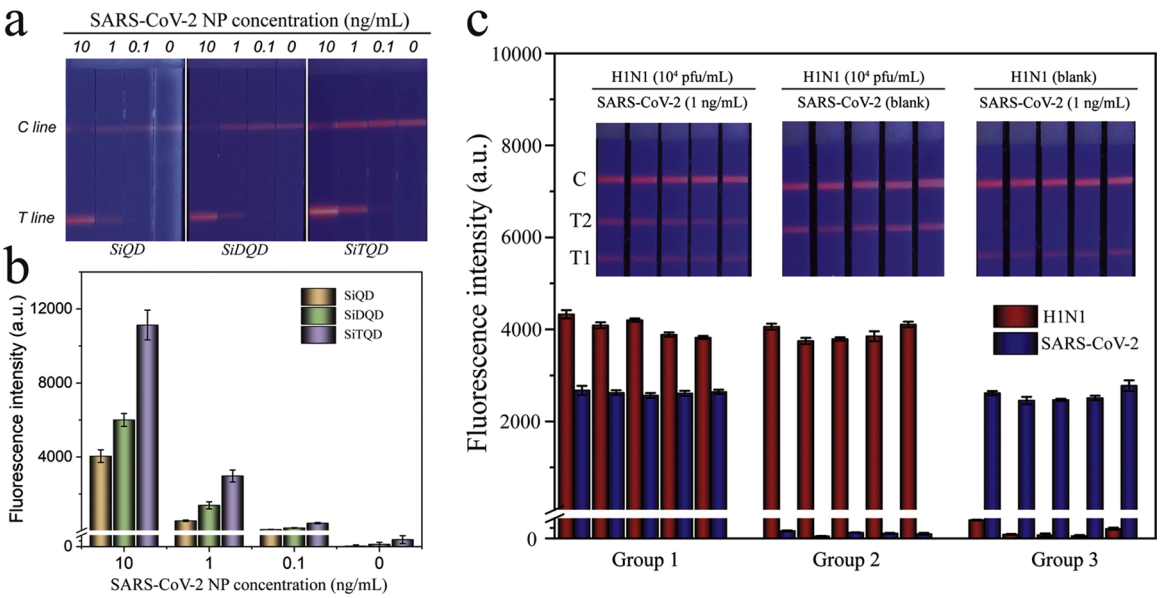

Fig. 4. (a) Fluorescence pictures and (b) corresponding test line intensities of the SiQD-ICA, SiDQD-ICA and SiTQD-ICA strips for SARS-CoV-2 NP antigen detection. (c) Reproducibility of the SiTQD-ICA for H1N1 and SARS-CoV-2 NP.

to define the limits of detection (LODs) of the ICA, where y_{blank} and SD_{blank} are the average fluorescence intensity and standard deviation of the blank groups, respectively [51–53]. Thus, the LOD values for SARS-CoV-2 NP and H1N1 were estimated as 5 pg/mL and 50 pfu/mL in this assay.

As a sensitive POCT tool for respiratory viruses, the performance of SiTQD-ICA should be compared with the traditional AuNP-based ICA strips, which used the same pairs of mAbs. The preparation of AuNP-based ICA was provided in Supporting information S2. As displayed in Fig. 3d, the visual sensitivity levels based on the naked eye of AuNP-based ICA strips for H1N1 and SARS-CoV-2 NP were 5000 pfu/mL and 1 ng/mL. By comparison, the sensitivity of SiTQD-ICA for target virus detection was at least 100 times higher than that of the AuNP-ICA based method. We further compared the testing ability of our method and commercially available ELISA kits. The ELISA analysis for SARS-CoV-2 NP and H1N1 was carried out with the instructions of manufacturer, and the detection results are displayed in Fig. 3e-f. By recording the absorbance at 450 nm with a microplate reader, the LODs determined by the ELISA kits for SARS-CoV-2 NP and H1N1 were 0.1 ng/mL and 5000 pfu/mL, respectively. Thus, we can conclude that our SiTQD-ICA strip is 20 and 100 times more sensitive than ELISA methods for SARS-CoV-2 NP and H1N1, respectively. In view of the long testing time (2–3 h) and cumbersome operation of ELISA assays, our method could be completed within 15 min and does not need large equipment and skilled personnel and is thus more suitable for rapid and sensitive screening of clinical samples.

The high sensitivity of the proposed method can be attributed to the high performance of SiTQD labels used. Comparison between the proposed SiTQD-ICA and two other kinds of Si-QD (SiQD and SiDQD)-based ICA was performed to verify the advantage of SiTQD with triple layers of QD shell for fluorescence signal amplification. Fig. 4a shows the fluorescence images of SiQD-ICA, SiDQD-ICA, and SiTQD-ICA for testing SARS-CoV-2 NP in different concentrations (10–0.1 ng/mL). The tested strips of SiTQD-ICA showed higher distinguishable SARS-CoV-2 levels by eye observation. Moreover, the fluorescence intensity values of both T/C lines of SiTQD-ICA strips were much higher than those of SiQD-ICA and SiDQD-ICA (Fig. 4b). The results confirmed that using SiTQD QBs with superior performance can improve the detection sensitivity of ICA biosensor. In addition, the SiTQD with a huge SiO_2 core ensured its monodispersity and excellent stability in sample solution, which benefit the reproducibility of the ICA. As revealed in Fig. 4c, the two-channel

Table 1
Recovery results for SARS-CoV-2 NP and H1N1 virions spiked in throat swab samples.

Target	Added concentration	Detected concentration	Recovery (%)	CV (%)
SARS-CoV-2 NP (ng/mL)	2000	2048.9	102.4	4.30
	1000	1108.2	110.8	6.53
	500	497.1	99.4	6.21
	100	97.7	97.7	4.61
	1	0.955	95.5	3.64
FluA H1N1 (pfu/mL)	0.5	0.563	112.6	4.39
	0.1	0.091	91.6	9.39
	0.05	0.057	114.4	4.25

SiTQD-ICA exhibited good fluorescence signal reproducibility on the T lines for one virus testing or simultaneous detection of two target viruses. The coefficients of variation (CV) for the fluorescence signals of T1 and T2 lines are below 4.3 % and 2.76 %, respectively, suggesting the high reliability of our method. Different concentrations of H1N1 virions (2000-100 pfu/mL) and SARS-CoV-2 NP (1-0.05 ng/mL) were spiked into the throat swab samples and tested by SiTQD-ICA to further assess the precision of our method. As demonstrated in Table 1, the average recoveries of our ICA biosensor ranged from 91.6% to 114.4% for H1N1 samples and ranged from 97.7% to 110.8% for SARS-CoV-2 NP samples, respectively, with a relative low CV ranging from 3.64 % to 9.39 %. These results indicated the acceptable accuracy of SiTQD-ICA for quantification of two target viruses.

The specificity of the SiTQD-ICA was assessed against other respiratory viruses including highly pathogenic coronaviruses (SARS-CoV and MERS-CoV), common human coronavirus (HCoV-HKU1), FluB, human adenovirus (HAdV), and RSV. In brief, 10^6 pfu/mL of inactivated virus samples (FluB, HAdV, RSV) and 1000 ng/mL coronavirus NP samples (SARS-CoV NP, MERS-CoV NP, HCoV-HKU1) were detected by our proposed method (Fig. 5a). A weak fluorescence band on the T1 line for the SARS-CoV NP group was observed, whereas other control samples exhibited no perceivable fluorescence signal on the T zones. As predicted, the SARS-CoV-2 NP and H1N1 groups exhibited a distinct signal band on their corresponding T lines. These results demonstrated that the proposed assay has a weak cross reaction with SARS-CoV NP at high concentrations and can specifically distinguish SARS-CoV-2/H1N1 from other common respiratory viruses.

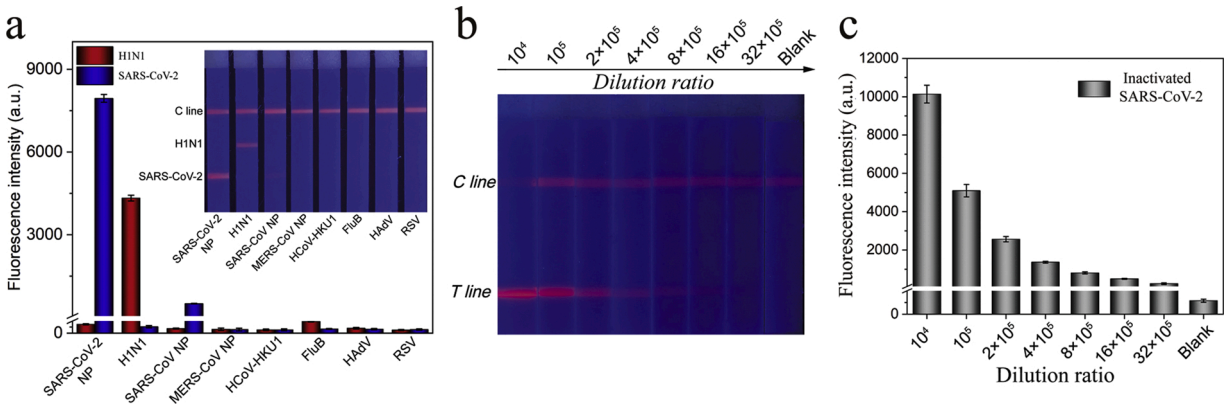

Fig. 5. (a) Specificity of SiTQD-based ICA. (b) Fluorescence pictures and (c) corresponding test line intensities of SiTQD-based ICA for inactivated SARS-CoV-2 samples. Error bars are calculated from three experiments.

To verify the actual testing capability of SARS-CoV-2, the inactivated SARS-CoV-2 virion sample (~10^8 pfu/mL) was obtained from Prof. Chengfeng Qin and tested via the SiTQD-ICA. As revealed in Fig. 5b-c, the fluorescence intensities on the T1 line gradually decreased with increasing dilution (10^4-32×10^5 times) of inactivated samples. The red fluorescence band on the T zone was visible at 1: 32×10^5 dilution of the inactivated SARS-CoV-2 sample. These results verified the high sensitivity of the SiTQD-ICA for detection of real SARS-CoV-2 virion. Further considering the advantages of low cost, highly stable, easy operation, multiplex detection capacity, and short testing time, the proposed method is a promising POCT tool for the rapid and accurate diagnosis of respiratory viruses in real specimens.

4. Conclusions

In this work, we proposed a novel fluorescent SiTQD-ICA for sensitive and simultaneous diagnosis of SARS-CoV-2 and FluA antigens and demonstrated its high performance (sensitivity, stability, specificity, and reproducibility) in biological samples. Highly luminescent and monodispersed SiTQD QB was fabricated by coating a three-layer QDs formed shell onto the 180 nm SiO_2 core via our proposed PEI-mediated LbL assembly method and introduced into ICA system as the advanced optical nanoprobe. Under the optimal conditions, the SiTQD-ICA simultaneously detected SARS-CoV-2 NP and FluA H1N1 in throat swab samples with LOD values of 5 pg/mL and 50 pfu/mL, respectively. The compared test results verified that the sensitivity of SiTQD-ICA was improved by about 100 times than that of traditional AuNP-based ICA method and over 20 times than that of ELISA kits. To the best of our knowledge, this work is the first to develop a two-channel ICA for simultaneous detection of SARS-CoV-2 and FluA. We believe that the proposed method could be an efficient POCT tool for direct, rapid, and accurate detection of pathogenic respiratory viruses.

CRediT authorship contribution statement

Chongwen Wang: Conceptualization, Writing - original draft, Writing - review & editing, Supervision. **Xingsheng Yang:** Methodology, Writing - original draft. **Shuai Zheng:** Methodology, Writing - original draft. **Xiaodan Cheng:** Methodology, Data curation. **Rui Xiao:** Writing - review & editing, Supervision. **Qingjun Li:** Methodology. **Wenqi Wang:** Methodology. **Xiaoxian Liu:** Methodology. **Shengqi Wang:** Funding acquisition, Writing - review & editing, Supervision.

Declaration of Competing Interest

The authors declare that they have no known competing financial interests or personal relationships that could have appeared to influence the work reported in this paper.

Acknowledgements

This study was supported by the National Natural Science Foundation of China (Grant no. 81830101), the National S&T Major Project for Infectious Diseases Control (Grant nos. 2018ZX10712001-010, 2018ZX10101003-001), and the Natural Science Foundation of Anhui Province (Grant no. 1908085QB85). The authors would like to thank Prof. Chengfeng Qin from Beijing Institute of Microbiology and Epidemiology for providing inactivated SARS-CoV-2 virions. We thank Beijing Zhongkebaice Technology Service Co., for helping to conduct SEM and TEM analysis.

Appendix A. Supplementary data

Supplementary material related to this article can be found, in the online version, at doi:https://doi.org/10.1016/j.snb.2021.130372.

References

[1] N.K. Singh, P. Ray, A.F. Carlin, C. Magallanes, S.C. Morgan, L.C. Laurent, et al., Hitting the diagnostic sweet spot: point-of-care SARS-CoV-2 salivary antigen testing with an off-the-shelf glucometer, Biosens. Bioelectron. 180 (2021), 113111.
[2] WHO. Coronavirus Disease 2019 (COVID-19): weekly epidemiological update. https://www.who.int/publications/m/item/weekly-epidemiological-update-on-covid-19—6-april-2021 (Accessed 6 April 2021).
[3] M. Patchsung, K. Jantarug, A. Pattama, K. Aphicho, S. Suraritdechachai, P. Meesawat, et al., Clinical validation of a Cas13-based assay for the detection of SARS-CoV-2 RNA, Nat. Biomed. Eng. 4 (2020) 1140–1149.
[4] R. Wölfel, V.M. Corman, W. Guggemos, M. Seilmaier, S. Zange, M.A. Müller, et al., Virological assessment of hospitalized patients with COVID-2019, Nature 581 (2020) 465–469.
[5] F. Cui, H.S. Zhou, Diagnostic methods and potential portable biosensors for coronavirus disease 2019, Biosens. Bioelectron. 165 (2020), 112349.
[6] D.J. Steiner, J.S. Cognetti, E.P. Luta, A.M. Klose, J. Bucukovski, M.R. Bryan, et al., Array-based analysis of SARS-CoV-2, other coronaviruses, and influenza antibodies in convalescent COVID-19 patients, Biosens. Bioelectron. 169 (2020), 112643.
[7] M.M. Azar, M.L. Landry, Detection of influenza A and B viruses and respiratory syncytial virus by use of clinical laboratory improvement amendments of 1988 (CLIA)-waived point-of-care assays: a paradigm shift to molecular tests, J. Clin. Microbiol. 56 (2018) e00367–18.
[8] Y. Yao, X. Chen, X. Zhang, Q. Liu, J. Zhu, W. Zhao, et al., Rapid detection of influenza virus subtypes based on an integrated centrifugal disc, ACS Sens. 5 (2020) 1354–1362.
[9] Y. Wang, D. Liu, H. Lin, D. Chen, J. Sun, Y. Xie, et al., Development of a broadly applicable Cas12a-linked beam unlocking reaction for sensitive and specific detection of respiratory pathogens including SARS-CoV-2, ACS Chem. Biol. 16 (2021) 491–500.
[10] X. Wu, Y. Cai, X. Huang, X. Yu, L. Zhao, F. Wang, et al., Co-infection with SARS-CoV-2 and influenza a virus in patient with pneumonia, China, Emerg. Infect. Dis. 26 (2020) 1324–1326.
[11] M. Alafeef, K. Dighe, P. Moitra, D. Pan, Rapid, ultrasensitive, and quantitative detection of SARS-CoV-2 using antisense oligonucleotides directed electrochemical biosensor chip, ACS Nano 14 (2020) 17028–17045.

[12] L. Huang, L. Ding, J. Zhou, S. Chen, F. Chen, C. Zhao, et al., One-step rapid quantification of SARS-CoV-2 virus particles via low-cost nanoplasmonic sensors in generic microplate reader and point-of-care device, Biosens. Bioelectron. 171 (2021), 112685.
[13] B.D. Grant, C.E. Anderson, J.R. Williford, L.F. Alonzo, V.A. Glukhova, D.S. Boyle, et al., SARS-CoV-2 coronavirus nucleocapsid antigen-detecting half-strip lateral flow assay toward the development of point of care tests using commercially available reagents, Anal. Chem. 92 (2020) 11305–11309.
[14] M. Feng, J. Chen, J. Xun, R. Dai, W. Zhao, H. Lu, et al., Development of a sensitive immunochromatographic method using lanthanide fluorescent microsphere for rapid serodiagnosis of COVID-19, ACS Sens. 5 (2020) 2331–2337.
[15] Z. Chen, Z. Zhang, X. Zhai, Y. Li, L. Lin, H. Zhao, et al., Rapid and sensitive detection of anti-SARS-CoV-2 IgG, using lanthanide-doped nanoparticles-based lateral flow immunoassay, Anal. Chem. 92 (2020) 7226–7231.
[16] X. Zhu, X. Wang, L. Han, T. Chen, L. Wang, H. Li, et al., Multiplex reverse transcription loop-mediated isothermal amplification combined with nanoparticle-based lateral flow biosensor for the diagnosis of COVID-19, Biosens. Bioelectron. 166 (2020), 112437.
[17] N.C. Cady, N. Tokranova, A. Minor, N. Nikvand, K. Strle, W.T. Lee, et al., Multiplexed detection and quantification of human antibody response to COVID-19 infection using a plasmon enhanced biosensor platform, Biosens. Bioelectron. 171 (2021), 112679.
[18] Y. Orooji, H. Sohrabi, N. Hemmat, F. Oroojalian, B. Baradaran, A. Mokhtarzadeh, et al., An overview on SARS-CoV-2 (COVID-19) and other human coronaviruses and their detection capability via amplification assay, chemical sensing, biosensing, immunosensing, and clinical assays, Nanomicro Lett. 13 (2021) 18.
[19] G. Qiu, Z. Gai, Y. Tao, J. Schmitt, G.A. Kullak-Ublick, J. Wang, Dual-functional plasmonic photothermal biosensors for highly accurate severe acute respiratory syndrome coronavirus 2 detection, ACS Nano 14 (2020) 5268–5277.
[20] K. Kim, L. Kashefi-Kheyrabadi, Y. Joung, K. Kim, H. Dang, S.G. Chavan, et al., Recent advances in sensitive surface-enhanced Raman scattering-based lateral flow assay platforms for point-of-care diagnostics of infectious diseases, Sens. Actuators B-Chem. 329 (2021), 129214.
[21] Y. Zhou, Y. Chen, Y. Liu, H. Fang, X. Huang, Y. Leng, et al., Controlled copper in situ growth-amplified lateral flow sensors for sensitive, reliable, and field-deployable infectious disease diagnostics, Biosens. Bioelectron. 171 (2021), 112753.
[22] C. Parolo, A. Sena-Torralba, J.F. Bergua, E. Calucho, C. Fuentes-Chust, L. Hu, et al., Tutorial: design and fabrication of nanoparticle-based lateral-flow immunoassays, Nat. Protoc. 15 (2020) 3788–3816.
[23] D. Liu, C. Ju, C. Han, R. Shi, X. Chen, D. Duan, et al., Nanozyme chemiluminescence paper test for rapid and sensitive detection of SARS-CoV-2 antigen, Biosens. Bioelectron. 173 (2020), 112817.
[24] A.N. Baker, S.-J. Richards, C.S. Guy, T.R. Congdon, M. Hasan, A.J. Zwetsloot, et al., The SARS-COV-2 spike protein binds sialic acids and enables rapid detection in a lateral flow point of care diagnostic device, ACS Central Sci. 6 (2020) 2046–2052.
[25] T. Mahmoudi, M. de la Guardia, B. Baradaran, Lateral flow assays towards point-of-care cancer detection: a review of current progress and future trends, TrAC-Trend Anal. Chem. 125 (2020), 115842.
[26] S. Liu, L. Dou, X. Yao, W. Zhang, M. Zhao, X. Yin, et al., Nanozyme amplification mediated on-demand multiplex lateral flow immunoassay with dual-readout and broadened detection range, Biosens. Bioelectron. 169 (2020), 112610.
[27] Y. Shao, H. Duan, L. Guo, Y. Leng, W. Lai, Y. Xiong, Quantum dot nanobead-based multiplexed immunochromatographic assay for simultaneous detection of aflatoxin B1 and zearalenone, Anal. Chim. Acta 1025 (2018) 163–171.
[28] Z. Rong, Q. Wang, N. Sun, X. Jia, K. Wang, R. Xiao, et al., Smartphone-based fluorescent lateral flow immunoassay platform for highly sensitive point-of-care detection of Zika virus nonstructural protein 1, Anal. Chim. Acta 1055 (2019) 140–147.
[29] H. Li, B. Dong, L. Dou, W. Yu, X. Yu, K. Wen, et al., Fluorescent lateral flow immunoassay for highly sensitive detection of eight anticoagulant rodenticides based on cadmium-free quantum dot-encapsulated nanospheres, Sens. Actuators B-Chem. 324 (2020), 128771.
[30] H. Duan, Y. Li, Y. Shao, X. Huang, Y. Xiong, Multicolor quantum dot nanobeads for simultaneous multiplex immunochromatographic detection of mycotoxins in maize, Sens. Actuators B-Chem. 291 (2019) 411–417.
[31] L. Huang, J. Jin, L. Ao, C. Jiang, Y. Zhang, H.M. Wen, et al., Hierarchical plasmonic-fluorescent labels for highly sensitive lateral flow immunoassay with flexible dual-modal switching, ACS Appl. Mater. Interfaces 12 (2020) 58149–58160.
[32] J. Hu, Z.L. Zhang, C.Y. Wen, M. Tang, L.L. Wu, C. Liu, et al., Sensitive and quantitative detection of C-reaction protein based on immunofluorescent nanospheres coupled with lateral flow test strip, Anal. Chem. 88 (2016) 6577–6584.
[33] S.J. Yeo, H. Kang, T.D. Dao, B.T. Cuc, A.T.V. Nguyen, T.T.T. Tien, et al., Development of a smartphone-based rapid dual fluorescent diagnostic system for the simultaneous detection of influenza A and H5 subtype in avian influenza A-infected patients, Theranostics 8 (2018) 6132–6148.
[34] J. Li, Y. Lv, N. Li, R. Wu, M. Xing, H. Shen, et al., Robust synthesis of bright multiple quantum dot-embedded nanobeads and its application to quantitative immunoassay, Chem. Eng. J. 361 (2019) 499–507.
[35] L. Huang, T. Liao, J. Wang, L. Ao, W. Su, J. Hu, Brilliant pitaya-type silica colloids with central–radial and high-density quantum dots incorporation for ultrasensitive fluorescence immunoassays, Adv. Funct. Mater. 28 (2018), 1705380.
[36] C. Wang, C. Wang, X. Wang, K. Wang, Y. Zhu, Z. Rong, et al., Magnetic SERS strip for sensitive and simultaneous detection of respiratory viruses, ACS Appl. Mater. Interfaces 11 (2019) 19495–19505.
[37] N.N. Zhang, X.F. Li, Y.Q. Deng, H. Zhao, Y.J. Huang, G. Yang, et al., A thermostable mRNA vaccine against COVID-19, Cell 182 (2020) 1271–1283, e16.
[38] Y. Li, J. Li, Y. Zhang, L. Dai, L. Li, J. Liu, et al., Development of an automatic integrated gene detection system for novel severe acute respiratory syndrome-related coronavirus (SARS-CoV2), Emerg. Microbes Infect. 9 (2020) 1489–1496.
[39] H. Li, C. Zhao, Y. Zhang, F. Yuan, Q. Zhang, X. Shi, et al., Establishment of replication-competent vesicular stomatitis virus-based recombinant viruses suitable for SARS-CoV-2 entry and neutralization assays, Emerg. Microbes Infect. 9 (2020) 2269–2277.
[40] X. Yang, X. Liu, B. Gu, H. Liu, R. Xiao, C. Wang, et al., Quantitative and simultaneous detection of two inflammation biomarkers via a fluorescent lateral flow immunoassay using dual-color SiO2@QD nanotags, Microchim. Acta 187 (2020) 570.
[41] C. Wang, X. Yang, B. Gu, H. Liu, Z. Zhou, L. Shi, et al., Sensitive and simultaneous detection of SARS-CoV-2-specific IgM/IgG using lateral flow immunoassay based on dual-mode quantum dot nanobeads, Anal. Chem. 92 (2020) 15542–15549.
[42] C. Wang, W. Shen, Z. Rong, X. Liu, B. Gu, R. Xiao, et al., Layer-by-layer assembly of magnetic-core dual quantum dot-shell nanocomposites for fluorescence lateral flow detection of bacteria, Nanoscale 12 (2020) 795–807.
[43] X. Liu, X. Yang, K. Li, H. Liu, R. Xiao, W. Wang, et al., Fe3O4@Au SERS tags-based lateral flow assay for simultaneous detection of serum amyloid A and C-reactive protein in unprocessed blood sample, Sens. Actuators B-Chem. 320 (2020), 128350.
[44] Z. Bai, H. Wei, X. Yang, Y. Zhu, Y. Peng, J. Yang, et al., Rapid enrichment and ultrasensitive detection of influenza a virus in human specimen using magnetic quantum dot nanobeads based test strips, Sens. Actuators B-Chem. 325 (2020), 128780.
[45] C. Wang, R. Xiao, S. Wang, X. Yang, Z. Bai, X. Li, et al., Magnetic quantum dot based lateral flow assay biosensor for multiplex and sensitive detection of protein toxins in food samples, Biosens. Bioelectron. 146 (2019), 111754.
[46] Z. Rong, Z. Bai, J. Li, H. Tang, T. Shen, Q. Wang, et al., Dual-color magnetic-quantum dot nanobeads as versatile fluorescent probes in test strip for simultaneous point-of-care detection of free and complexed prostate-specific antigen, Biosens. Bioelectron. 145 (2019), 111719.
[47] H. Liu, E. Dai, R. Xiao, Z. Zhou, M. Zhang, Z. Bai, et al., Development of a SERS-based lateral flow immunoassay for rapid and ultra-sensitive detection of anti-SARS-CoV-2 IgM/IgG in clinical samples, Sens. Actuators B-Chem. 329 (2021), 129196.
[48] X. Ou, Y. Liu, X. Lei, P. Li, D. Mi, L. Ren, et al., Characterization of spike glycoprotein of SARS-CoV-2 on virus entry and its immune cross-reactivity with SARS-CoV, Nat. Commun. 11 (2020) 1620.
[49] G.M.S. Ross, D. Filippini, M.W.F. Nielen, G.I. Salentijn, Unraveling the hook effect: a comprehensive study of high antigen concentration effects in sandwich lateral flow immunoassays, Anal. Chem. 92 (2020) 15587–15595.
[50] W. Chen, S. Shan, J. Peng, D. Liu, J. Xia, B. Shao, et al., Sensitive and hook effect–free lateral flow assay integrated with cascade signal transduction system, Sens. Actuators B-Chem. 321 (2020), 128465.
[51] X. Wang, N. Choi, Z. Cheng, J. Ko, L. Chen, J. Choo, Simultaneous detection of dual nucleic acids using a SERS-based lateral flow assay biosensor, Anal. Chem. 89 (2017) 1163–1169.
[52] D. Zhang, L. Huang, B. Liu, H. Ni, L. Sun, E. Su, et al., Quantitative and ultrasensitive detection of multiplex cardiac biomarkers in lateral flow assay with core-shell SERS nanotags, Biosens. Bioelectron. 106 (2018) 204–211.
[53] J. Hu, Y.Z. Jiang, L.L. Wu, Z. Wu, Y. Bi, G. Wong, et al., Dual-signal readout nanospheres for rapid point-of-care detection of ebola virus glycoprotein, Anal. Chem. 89 (2017) 13105–13111.

Chongwen Wang is currently a professor at Anhui Agricultural University in China. His work focuses on the preparation and application of novel metal and magnetic nanomaterials.

Xingsheng Yang is a master student under the guidance of Prof. Chongwen Wang at Anhui Agricultural University in China. His work focuses on the development of ICA-based biosensors.

Shuai Zheng is a currently a doctoral candidate under the guidance of Prof. Rui Xiao at Anhui Agricultural University in China. His work focuses on the development of POCT methods.

Xiaodan Cheng is a master student under the guidance of Prof. Chongwen Wang at Anhui Agricultural University in China. Her work focuses on the development of ICA-based biosensors.

Rui Xiao is currently a professor at the Beijing Institute of Radiation Medicine. Her research interests include SERS-based biosensor and nanomaterials-based sensors.

Qingjun Li is a currently a doctoral candidate under the guidance of Prof. Shengqi Wang at Shandong University of Traditional Chinese Medicine in China. His work focuses on the development of detection method for viruses.

Wenqi Wang is a master student under the guidance of Prof. Chongwen Wang at Anhui Agricultural University in China. His work focuses on the development of ICA-based biosensors.

Xiaoxian Liu is a technicist in Beijing Institute of Radiation Medicine in China. Her work focuses on the development of fluorescent biosensors.

Shengqi Wang is currently a professor at the Beijing Institute of Radiation Medicine. His research interests include DNA/protein biosensing, virology, and pharmacology.